JCTC Journal of Chemical Theory and Computation

ARTICLE

pubs.acs.org/JCTC

Solvent Effects on the Structure and Spectroscopy of the Emitting States of 1-Phenylpyrrole

Ignacio Fdez. Galván,* M. Elena Martín, Aurora Muñoz-Losa, M. Luz Sánchez, and Manuel A. Aguilar

Química Física, Edif. José María Viguera Lobo, Universidad de Extremadura, Avda. de Elvas s/n, 06071 Badajoz, Spain

ABSTRACT: Theoretical calculations of absorption and fluorescence properties of 1-phenylpyrrole have been performed, at the CASPT2//CASSCF level, in the gas phase and in acetonitrile solution, using in the latter case the ASEP/MD method. In addition to a locally excited state, it was also possible to identify a candidate intramolecular charge transfer state that could explain the second red-shifted fluorescence band that appears in polar solvents. In the gas phase, the charge transfer state is found to lie higher in energy than the locally excited state and the Franck−Condon absorption state, making it unlikely to be reached under these conditions. In acetonitrile solution, the charge transfer state is stabilized and lies much closer to the locally excited state, becoming accessible after absorption. The results indicate that the free-energy surface of the charge transfer state is very flat in solution, and several geometries are possible, ranging from almost planar to twisted and bent. Solvent caging and transition probabilities favor emission from structures with a small twist angle between the rings and without a pyramidal atom.

1. INTRODUCTION

A significant number of organic molecules combining electron donor and acceptor groups exhibit the so-called dual fluorescence in polar solvents. In nonpolar solvents, the fluorescence spectrum features a single "normal" band, which suffers only a slight shift when the solvent polarity is increased. In polar solvents, a second "anomalous" band appears in the spectrum; this second band's position and intensity is much more affected by the solvent polarity, being strongly red-shifted and intensified (at the expense of the "normal" band) in highly polar solvents. The phenomenon of dual fluorescence has been widely studied in the literature since its discovery 50 years ago.[1−8] It was suggested early on that the "anomalous" fluorescence band is due to the existence of an intramolecular charge transfer (ICT) state that can be stabilized in polar solvents, while in nonpolar solvents only the state responsible for the "normal" band, usually called local excitation (LE), is stable enough to be observed.

This picture is still generally accepted as a valid explanation for the dual fluorescence. However, there is a continuing controversy between different groups regarding the nature and geometry of the ICT state, the possible existence of other intermediate states, the mechanism through which the LE and ICT states are formed, and practically every other detail of the dual fluorescence phenomenon.

Perhaps the most successful models for the dual fluorescence in the prototype molecule 4-(N,N-dimethylamino)benzonitrile (DMABN) and its derivatives are the ones known as TICT (twisted ICT) and PICT (planar ICT). These models propose, respectively, a perpendicular and coplanar relative configuration of the donor and acceptor groups. Experimental evidence in favor of one model or the other is usually derived from comparison of the properties of various compounds with different geometric constraints and substituents. For example, compounds like 3,5-dimethyl-4-(N,N-dimethylamino)benzonitrile, where the dimetylamino group is forced to be twisted, display only the ICT band in fluorescence, suggesting a TICT is responsible for the band. Other compounds where the twisting is hindered (like 6-cyano-1,2,3,4-tetrahydroquinoline, NTC6) can present dual fluorescence, which points to a PICT state. These apparently conflicting conclusions probably indicate that the two models can be valid, and each particular system will favor one of them.

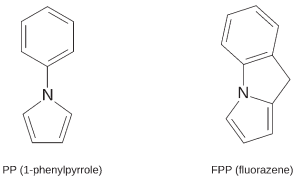

Figure 1. Two similar compounds with dual fluorescence.

In recent years, a pair of closely related molecules has been studied for their dual fluorescence properties, see Figure 1. The two rings in 1-phenylpyrrole (PP) can freely rotate around the middle bond, while fluorazene (FPP) has a methylene bridge that effectively locks the rings in an almost planar conformation. Interestingly, both molecules have very similar photophysical properties, and in particular, both show dual fluorescence in polar solvents. Moreover, the planar FPP has been found to have enhanced ICT emission compared to PP (it appears in less polar solvents and has a higher quantum yield), which naturally leads to the conclusion that the PICT model applies better to these molecules.[9,10] However, most theoretical calculations predict a twisted structure for the ICT state of PP,[11−15] which seems unsatisfactory.

In this work, we have carried out a theoretical study on the absorption and fluorescence properties of the PP molecule, both in the gas phase and in acetonitrile solution. The electronic states of PP are described with a multiconfigurational quantum method, and we used an explicit model of atomic detail for the solvent. By examining

Received: February 18, 2011
Published: April 29, 2011

the relative energies, geometries, and emission energies of the different electronic states, we hope to cast further light on the nature of the emitting ICT state of this interesting system.

Early during this research, it became evident that we were not getting "ideal" TICT or PICT structures, and that this nomenclature would not be adequate to describe the results. Therefore, in the rest of this paper, we have avoided the use of these two terms, preferring other descriptive terms for the ICT state and its geometries.

2. METHODS AND DETAILS

Solvent effects on the PP UV/vis spectra were calculated with the ASEP/MD (Average Solvent Electrostatic Potential from Molecular Dynamics) method. This is a sequential quantum mechanics/molecular mechanics (QM/MM) method implementing the mean field approximation. It combines, alternately, a high-level quantum mechanics (QM) description of the solute with a classical molecular mechanics (MM) description of the solvent. One of its main features is the fact that the solvent effect is introduced into the solute's wave function as an average perturbation. Details of the method have been described in previous papers,[16−18] so here we will only present a brief outline.

As mentioned above, ASEP/MD is a method combining QM and MM techniques, with the particularity that full QM and MD (molecular dynamics) calculations are alternated and not simultaneous. During the MD simulations, the intramolecular geometry and charge distribution of all molecules, and particularly the solute, is considered fixed. From the resulting simulation data, the average electrostatic potential generated by the solvent molecules on the solute (ASEP) is obtained. This potential is introduced as a perturbation into the solute's quantum mechanical Hamiltonian, and by solving the associated Schrödinger equation, one gets a new charge distribution for the solute, which is used in the next MD simulation. This iterative process is repeated until the electron distribution of the solute and the solvent structure around it are mutually equilibrated.

The ASEP/MD framework can also be used to optimize the geometry of the solute molecule.[19] At each step of the ASEP/MD procedure, the gradient and Hessian on the system's free-energy surface (including the van der Waals contribution) can be obtained, and thus they can be used to search for stationary points on this surface by some optimization method. In the computation of the gradient and Hessian, the free-energy gradient method[20] is used, with the incorporation of the mean field approximation to reduce the number of quantum calculations needed. In this way, after each MD simulation, the solute geometry is optimized within the fixed "average" solvent structure by using the free-energy derivatives. In the next MD simulation, the new solute geometry and charge distribution are used. This approach allows the optimization of the solute geometry in parallel with the solvent structure.

For calculating transition energies, the iterative process is performed on the initial state of the transition (the ground state for absorption, the excited state for emission); i.e., the atomic charges for the MD and the energy derivatives for the geometry optimization of the solute are calculated with the initial state's wave function. Then, with a frozen solvent model, the transition energies between the different states are obtained.

Once the different solute electronic states and the solvent structure around them have been optimized and equilibrated, the free energy differences between those states can be calculated, within the ASEP/MD framework, making use of the free energy perturbation method.[21,22] The expression we use to calculate the free energy difference between two species in equilibrium in solution, ΔG, is

$$\Delta G = \Delta E + \Delta G_{\text{int}} + \Delta V \quad (1)$$

where ΔE is the difference in the internal quantum energy of the solute between the two species, ΔG_{int} is the difference in the solute−solvent interaction energy, which is calculated classicaly with the free energy perturbation method, and ΔV is a term that includes the difference in the zero-point energy (ZPE) and entropic contributions of the solute. The last term, ΔV, is normally evaluated by applying the harmonic approximation to the vibrational modes of the solute in solution, and it needs the information provided by the Hessian matrix. In this work, obtaining an accurate enough Hessian matrix required computational resources that were too large, and we decided to approximate the results by neglecting this term. It must be noted that this ΔV term refers only to the internal nuclear degrees of freedom of the solute; free energy contributions from the solvent around the solute are properly accounted for in the ΔG_{int} term.

2.1. Computational Details. The quantum calculations on the solute molecule were done with the complete active space self-consistent field (CASSCF) method,[23] using the 6-31G* basis set. In some cases, single-point calculations with the cc-pVTZ basis set were also performed. The active orbitals were the six π and π^* orbitals of the phenyl ring, plus the five π and π^* orbitals of the pyrrole ring, and 12 electrons were included in these orbitals, for a (12,11) total active space. All calculations were performed using a state-average (SA) of the first five singlet states, with equal weights. It is known that, in order to obtain accurate transition energies, it is necessary to include the dynamic electron correlation in the quantum calculations, which we did with the complete active space second order perturbation (CASPT2) method,[24,25] using the SA(5)-CASSCF(12,11) wave functions as a reference. An IPEA-shifted (ionization potential−electron affinity) zeroth-order Hamiltonian has been proposed for CASPT2 calculations,[26] which is supposed to reduce systematic overstabilization errors in open-shell systems (as is the case of the excited states studied here). We did all CASPT2 with the proposed IPEA shift of 0.25 E_h (CASPT2(0.25)) as well as with no IPEA shift (CASPT2(0.00)). To minimize the appearance of intruder states, an additional imaginary shift of 0.1 i E_h was used. No symmetry was imposed or assumed in any case.

The MD simulations were carried out with rigid molecules, with acetonitrile (CH_3CN) as a solvent. Lennard-Jones parameters and solvent atomic charges were taken from the OPLS-AA (Optimized Potentials for Liquid Simulations, all atoms) force field,[27] solute atomic charges were computed from the quantum calculations through a least-squares fit to the electrostatic potential obtained at the points where the solvent charges are located. The geometry of acetonitrile was optimized with the Becke's three-parameter Lee−Yang−Parr density functional (B3LYP) and the 6-311G** basis set. A total of 375 CH_3CN molecules and the solute were included at the experimental solvent density (779.3 kg/m^3). Periodic boundary conditions were applied, and spherical cutoffs were used to truncate the interatomic interactions at 12.75 Å. Long-range interactions were calculated using the Ewald sum technique. The temperature was fixed at 298.15 K by using the Nosé−Hoover thermostat. A time step of 0.5 fs was

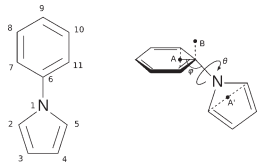

Figure 2. Atom numbering of the PP molecule and illustration of the two angles ϕ and θ.

Table 1. Definition of Geometric Parameters for the PP Molecule[a]

$\overline{\text{Ph}}$	$1/6(d(C_6C_7) + d(C_7C_8) + d(C_8C_9) + d(C_9C_{10}) + d(C_{10}C_{11}) + d(C_{11}C_6))$
$\overline{\text{Py}}$	$1/5(d(N_1C_2) + d(C_2C_3) + d(C_3C_4) + d(C_4C_5) + d(C_5N_1))$
$Q(\text{Ph})$	$1/4(d(C_6C_7) + d(C_8C_9) + d(C_9C_{10}) + d(C_{11}C_6)) - 1/2(d(C_7C_8) + d(C_{10}C_{11}))$
$Q(\text{Py})$	$1/3(d(N_1C_2) + d(C_3C_4) + d(C_5N_1)) - 1/2(d(C_2C_3) + d(C_4C_5))$
Ph−Py	$d(N_1C_6)$
ϕ	$a(AC_6N_1)$
ψ	$a(C_6N_1A')$
θ	$D(BC_6N_1B')$

[a] d is a bond length, a a bond angle, and D a dihedral angle. Point A is the midpoint between C_7 and C_{11}; point B is 1 Å away from C_6, in the normal direction of the $C_6C_7C_{11}$ plane. Points A′ and B′ are equivalent for the pyrrole ring. The angle ψ is always very close to 180°.

used during the simulations; each of them was run for 50 ps after 25 ps of equilibration.

At each step of the ASEP/MD procedure, 500 configurations evenly distributed from the MD run were used to calculate the ASEP. The charges from each solvent molecule were kept explicitly whenever the molecule's center of mass was closer than 9 a_0 to any solute nucleus; the effect of the farther molecules was included in an additional shell of fitted charges. Each ASEP/MD run was continued until the energies and solute geometry and charges were stabilized for at least five iterations; results are reported as the average of these last five iterations, being an effective average of 250 ps dynamics.

For in solution calculations, a development version of the ASEP/MD software[17] was used. All quantum calculations were performed with Molcas 6.4 and Molcas 7.4.[28] All MD simulations were performed using Moldy.[29] The electrostatic potential generated by the solute was calculated with Molden.[30]

3. RESULTS AND DISCUSSION

3.1. Gas Phase. *3.1.1. Optimized Geometries.* The PP geometry was optimized in the gas phase at the SA(5)-CASSCF-(12,11)/6-31G* level for the electronic ground state and different excited states. For comparing and describing the structures, we use some geometric parameters, such as the average bond length of the phenyl ring ($\overline{\text{Ph}}$), the average bond length of the pyrrole ring ($\overline{\text{Py}}$), the phenyl−pyrrole bond length (Ph−Py), or the phenyl−pyrrole twist angle (θ). See Figure 2 and Table 1 for the atom numbering and parameter definitions.

The optimized ground state (GS) structure features the usual aromatic bond lengths in benzene and pyrrole ($\overline{\text{Ph}}$ = 1.397 Å, $\overline{\text{Py}}$ = 1.385 Å) and a similar Ph−Py length of 1.400 Å. The N_1-C_6 bond is coplanar with both rings, and the twist angle θ takes a value of 29.7°. Similar geometries are found in the literature for theoretical calculations,[11−13,15,31,32] the θ angle ranging from 28° with AM1 to 42.7° with CASSCF(12,11)/6-31G*. The experimental determination of the twist angle in the gas phase yielded values of 32°[33] and 38.7°.[34] The pyrrole moiety is more electron-withdrawing than the phenyl, resulting in a slightly polarized electron density for the PP molecule, with a small global dipole moment of 1.48D.

At the ground state geometry, the first excited state corresponds to a $\pi \rightarrow \pi^*$ transition in the phenyl ring. When the geometry is optimized for this state, the LE (local excitation) geometry is reached. The rings in this geometry are also linear and slightly twisted. Ph−Py is shorter than for the GS (1.385 Å), and the θ angle is smaller too (20.9°). Reflecting the local excitation character of the state, $\overline{\text{Ph}}$ increases significantly to 1.432 Å. These features agree with other theoretical calculations, where the θ angle ranges from 1.95° with CIS/6-31+G** to 29.5° with CASSCF(12,11)/6-31G*,[15,32] although Zilberg and Haas reported a planar structure with θ = 0.0°.[13] The experimental data indicate that the optimum angle is 19.8°, but the rotation barrier is on the order of 0.3 kcal/mol.[34] The electron distribution in this state is similar to that of the ground state, and the dipole moment decreases to 0.40D.

In the higher excited states at the GS geometry, there is an intramolecular charge transfer. The electron density polarization is inverted with respect to the ground state, and the negative charge is displaced toward the phenyl ring, (see below, in section 3.1.2), which we indicate in the tables with a negative sign in the dipole moment. When the geometry of a charge transfer state is optimized in the gas phase, at least two different structures can be found. The lowest energy structure we could get has a pyramidalized C_6 atom, which is also slightly out of the main phenyl plane. The angle ϕ, which measures this pyramidalization of C_6, is 134.3°, while the twist angle θ is almost 90°. The deformation of the two rings is measured by their "quinoidality", defined in Table 1 as Q(Ph) and Q(Py), indicating the extent to which the C_7-C_8 and $C_{10}-C_{11}$ bonds are shorter (or longer, for negative Q) than the other bonds in the phenyl ring, and similarly for the pyrrole. In this case, Q(Ph) is 0.050 Å and Q(Py) is −0.085 Å, meaning that the C_7-C_8 and $C_{10}-C_{11}$ bonds become shorter while the C_2-C_3 and C_4-C_5 bonds become longer. The Ph−Py bond is longer than for the GS structure, 1.486 Å. At this geometry, the charge transfer state is the first excited singlet, S_1, and has a dipole moment of 8.21D. This bent twisted structure, which we will denote with PQ (perpendicular quinoidal), is also reported by Xu et al.,[15] and is found as well in calculations for the DMABN molecule.[35,36]

In the other structure, we find for the ICT state, the two rings remain almost linear, with a ϕ angle close to 180°, and the twist angle θ, instead of becoming perpendicular, decreases from the GS structure to 16.1°. In general, this structure, which we will call LQ (linear quinoidal), is similar to the GS and LE structures, with a shorter Ph−Py length (1.373 Å) and quinoidal and antiquinoidal phenyl and pyrrole rings, respectively (Q(Ph) = 0.074 Å, Q(Py) =− 0.093 Å). At this geometry, the ICT state is not the first but the second excited state, S_2 (although very close to S_1), and its dipole moment is lower than for the PQ, 4.67D, but in the same direction. A similar structure is reported by Zilberg and Haas,[13] although they use planar symmetry and give a very low dipole moment for it, 0.75D; this smaller value may be due to the presence of the S_1 state very close in energy, and to a different

Table 2. Geometrical Parameters and Dipole Moments of the Different Optimized Structures of PP in the Gas Phase[a]

	GS (S_0)	LE (S_1)	PQ (S_1)	LQ (S_2)
$\overline{\text{Ph}}$ (Å)	1.397	1.432	1.417	1.420
$\overline{\text{Py}}$ (Å)	1.385	1.387	1.389	1.405
Q(Ph) (Å)	0.004	−0.003	0.050	0.074
Q(Py) (Å)	0.025	0.035	−0.085	−0.093
Ph−Py (Å)	1.400	1.385	1.486	1.373
$180 - \phi$ (Å)	0.0	0.0	45.7	3.1
θ (deg)	29.7	20.9	89.6	16.1
μ (D)	1.48	0.40	−8.21	−4.67

[a] Geometries optimized at the SA-CASSCF level, dipoles calculated at the CASPT2(0.25) level. The negative sign in the dipole indicates the negative charge is displaced towards the phenyl ring.

Table 3. Vertical Absorption Energies (in eV), Dipole Moments (in D), and Oscillator Strengths for the PP Molecule in Gas Phase at the GS Geometry[a]

	vertical energies					
	CASSCF	CASPT2(0.25)	CASPT2(0.00)	exp.[39]	μ	f
S_0					1.48	
S_1	4.77	4.85	4.51		0.59	0.004
S_2	6.04	5.48	5.05	5.03	−3.43	0.436
S_3	6.13	5.84	5.53		−7.15	0.012
S_4	6.61	6.20	5.92		−10.09	0.037

[a] Dipole moments and oscillator strengths calculated at the CASPT2-(0.25) level. The negative sign in the dipole indicates the negative charge is displaced towards the phenyl ring.

state-averaging in their calculations. A summary of the different structures optimized in the gas phase is provided in Table 2.

Other authors have reported antiquinoidal structures for a charge transfer state,[13,14,37] where the C_7-C_8 and $C_{10}-C_{11}$ bonds are longer than other phenyl ring bonds, and therefore Q(Ph) is negative. We have, however, been unable to obtain such structures, all trials reverting to one of the quinoidal or LE geometries.

3.1.2. Absorption. The vertical absorption properties of PP at the optimized ground state geometry are summarized in Table 3. We report the CASSCF transition energies for comparison, but it is known that only transition energies calculated with dynamic electron correlation are reliable. Therefore, we will only discuss CASPT2 energies in the rest of the article. By comparing the CASPT2(0.25) and CASPT2(0.00) columns, it is ascertained that the former values are always 0.3−0.4 eV larger; this difference has been found in previous works.[35,38] Other properties like dipole moments or oscillator strengths are much more similar between the two CASPT2 variants, and only CASPT2(0.25) values are reported. Of the four transitions studied, only $S_0 \rightarrow S_2$ has a relatively large oscillator strength and is therefore predicted to be the active transition in the absorption spectrum. The experimental spectrum shows a broad band at 5.03 eV,[39] and in some solvents a weak shoulder appears in the red end, indicating the presence of a hidden band. Thus, the experimental absorption can be safely assigned to the $S_0 \rightarrow S_2$ transition.

As previously found, the CASPT2(0.00) values with the 6-31G* basis set tend to agree very well with the experiment,

Table 4. Same as Table 3, with the cc-pVTZ//6-31G* Basis Set

	vertical energies				
	CASSCF	CASPT2(0.25)	CASPT2(0.00)	μ	f
S_0				1.50	
S_1	4.72	4.71	4.28	0.42	0.004
S_2	5.89	5.20	4.71	−3.83	0.449
S_3	5.96	5.57	5.21	−7.41	0.012
S_4	6.37	5.85	5.49	−10.08	0.061

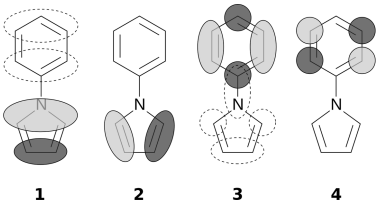

Figure 3. Main active molecular π orbitals of PP (simplified). Dashed contributions appear in more planar structures (lower θ). In the dominant ground state configuration, orbitals 1 and 2 are doubly occupied, while 3 and 4 are empty ($1^2 2^2 3^0 4^0$).

while CASPT2(0.25) values are overestimated. This has been attributed to an error cancellation in the case of CASPT2(0.00), since in general, when increasing the basis set quality, transition energies decrease, and then, with larger basis sets, the CASPT2(0.25) results are closer to experimental results and CASPT2(0.00) results are underestimated. This can be confirmed in Table 4, where we show the results of calculations performed with the cc-pVTZ basis set on the same geometries obtained with 6-31G*. Other authors have also found that CASPT2(0.25) results are more robust and in better agreement with other comparable methods.[40] In view of these facts, we will generally report CASPT2(0.25) values, bearing in mind that transition energies are probably overestimated by around 0.4 eV due to the limited basis set employed. One should also be cautious when comparing with CASPT2 results reported in the bibliography, for many of them use the CASPT2(0.00) or similar variant.

When the electron configurations of the states are examined, it is clear that states S_3 and S_4 correspond mainly to single excitations from the pyrrole to the phenyl ring. In terms of the simplified molecular orbitals pictured in Figure 3, S_3 is a $2 \rightarrow 3$ transition, and S_4 is $2 \rightarrow 4$. S_1 has a significant contribution from other orbitals, resulting in a $\pi \rightarrow \pi^*$ transition local to the phenyl ring, while S_2 has the larger contribution from $1 \rightarrow 3$, but there is significant mixture of other transitions. It is interesting to note that, although the absorption to the S_2 state is the active one and this state has an evident charge transfer character, the optimized ICT structures detailed above (PQ and LQ) correspond to the electron configuration of S_3 ($2 \rightarrow 3$), as suggested by the values of Q(Ph) and Q(Py).

The energies and electron configurations of the states at the GS geometry are in good agreement with previous calculations by other groups,[11,12,14,15] although the DFT/MRCI method gives relatively lower energies for the S_3 and S_4 states.

3.1.3. Fluorescence. Experimentally, a single fluorescence band, assigned to the LE state, is observed in the gas phase or

Table 5. Vertical Emission Energies (Transitions to S_0, in eV), Dipole Moments (in D), and Oscillator Strengths for the PP Molecule in the Gas Phase[a]

	vertical energies				
	CASPT2(0.25)	CASPT2(0.00)	μ	f	ΔE
LE (S_1)	4.45	4.12	0.40	0.005	4.67
PQ (S_1)	3.80	3.55	−8.21	0.001	5.12
LQ (S_2)	4.71	4.41	−4.67	0.011	5.42

[a] ΔE is the relative energy (in eV) with respect to S_0 at the ground state minimum, GS. Dipole moments, oscillator strengths, and ΔE calculated at the CASPT2(0.25) level. The negative sign in the dipole indicates the negative charge is displaced towards the phenyl ring.

nonpolar solvents,[10,34,39,41,42] with a maximum at around 4.10−4.15 eV. In Table 5, we have summarized the calculated emission properties from the three excited-state structures obtained. The predicted LE fluorescence agrees very well with the experimental value, as does the Stokes shift, and the low oscillator strength is in accord with the findings of Belau et al.,[43] who conclude that the observed fluorescence occurs from a state different from that populated at excitation. The two charge transfer geometries have very different fluorescence properties: emission from the charge transfer state in PQ is around 0.9 eV lower in energy than in LQ, and its oscillator strength is significantly weaker. The ΔE values indicate that, while all three states are below the Franck−Condon absorption to S_2 (5.48 eV, see Table 3), only LE has a lower energy than S_1 at the GS structure (4.85 eV). This may explain why a single fluorescence band, corresponding to LE, is observed in the gas phase. The ΔE value for the LE structure, 4.67 eV, can be compared with the experimental 0−0 transition which is found at around 4.40 eV.[34] A scheme of the relative energies of the states at the different geometries is presented in Figure 4.

As happened in the case of absorption, calculations with the cc-pVTZ basis set yield lower transition energies by around 0.2 eV and make the CASPT2(0.00) values underestimated with respect to the experimental results. For comparison, cc-pVTZ result are given in Table 6.

3.2. Acetonitrile Solution. *3.2.1. Optimized Geometries.* The same structures obtained in the gas phase for the PP molecule were also optimized in acetonitrile solution, using the ASEP/MD method[16−18] to model the solvation. The resulting geometries are given in Table 7. In the case of the LQ structure, it was not found to be a minimum but yielded the BQ structure when fully optimized (see below). The reported LQ geometry in solution corresponds to an optimization with the $C_8-C_7-C_6-N_1$ and $C_{10}-C_{11}-C_6-N_1$ dihedrals fixed to the ground state geometry values (an unconstrained optimization from the Franck−Condon point proceeds first to LQ and then to BQ).

The GS and LE geometries are hardly affected by the solvent, and only a small increase in the dipole moment is observed. The charge transfer structures PQ and LQ, as expected, suffer more significant changes. The ϕ angle in PQ becomes more linear, and the θ angle in LQ becomes more planar. The bond lengths are more similar between both structures than in the gas phase. The dipole moments are also quite similar and greatly enhanced from the gas phase values. These findings are in agreement with results obtained with the PCM method.[15]

In solution, we found another optimized structure for a charge transfer state, characterized by pyramidal C_6, like PQ, but with a nonperpendicular θ; this structure will be called BQ (bent quinoidal). In Table 7, it can be seen that the bond lengths and dipole moment are rather similar to PQ and LQ. The optimized charge transfer state in all three quinoidal structures obtained (PQ, LQ, and BQ) is dominated by the single excitation $2 \rightarrow 3$ (see Figure 3), suggesting that they belong to the same electronic energy surface. As in the gas phase calculations, we could not obtain an optimized geometry of antiquinoidal (negative Q(Ph)) character.

Table 6. Same as Table 5, with the cc-pVTZ//6-31G* Basis Set

	vertical energies			
	CASPT2(0.25)	CASPT2(0.00)	f	ΔE
LE (S_1)	4.32	3.90	0.005	4.56
PQ (S_1)	3.64	3.34	0.001	5.04
LQ (S_2)	4.52[a]	4.15	0.010	5.22

[a] At this level, the charge transfer state is S_1.

Table 7. Geometrical Parameters and Dipole Moments of the Different Optimized Structures of PP in Acetonitrile Solution[a]

	GS (S_0)	LE (S_1)	PQ (S_1)	LQ (S_1)[b]	BQ (S_1)
$\overline{\text{Ph}}$ (Å)	1.397	1.432	1.415	1.415	1.415
$\overline{\text{Py}}$ (Å)	1.385	1.387	1.388	1.393	1.391
Q(Ph) (Å)	0.004	−0.003	0.056	0.063	0.061
Q(Py) (Å)	0.023	0.034	−0.092	−0.095	−0.096
Ph-Py (Å)	1.404	1.386	1.468	1.417	1.446
$180 - \phi$ (°)	0.1	0.1	36.5	1.3	32.0
θ (°)	29.4	19.0	87.0	32.7	41.7
μ (D)	1.96	0.56	−11.92	−10.79	−10.91

[a] Geometries optimized at the SA-CASSCF level; dipoles calculated at CASPT2(0.25) level. The negative sign in the dipole indicates the negative charge is displaced towards the phenyl ring. [b] Not a fully optimized minimum, see the text.

3.2.2. Absorption. The results for ground state absorption properties of PP in CH_3CN are summarized in Table 8. The values obtained are very similar to those in the gas phase, with a small blue shift in the transition energies. The dipole moments of the S_0 and S_1 states are slightly increased, while the dipoles decrease for the other states due to their opposite direction. The calculated solvatochromic shift, 0.07 eV, contrasts with the experimental shift, −0.12 eV. A similar discrepancy was found in DMA (N,N-dimethylaniline) and DMABN,[35,38] and we attribute it to the neglect of the dispersion component in the electron transition energies. The dispersion component is expected to be quite uniform among solvents of similar refractive indexes, such as hexane (n = 1.375) and acetonitrile (n = 1.342). By comparing the transition energies in the gas phase (5.03 eV) and in hexane (4.87 eV),[10] we can get an estimation for the dispersion contribution to the solvatochromic shift. If this estimation (−0.16 eV) is added to the calculated gas−acetonitrile shift, an almost perfect agreement with experimental results is obtained. Otherwise, the blue shift in a vertical transition can be expected, in view of the opposite direction of the dipole moments in the S_0 and S_2 states.

3.2.3. Fluorescence. The calculated emission energies from the different optimized excited states in solution are shown in Table 9.

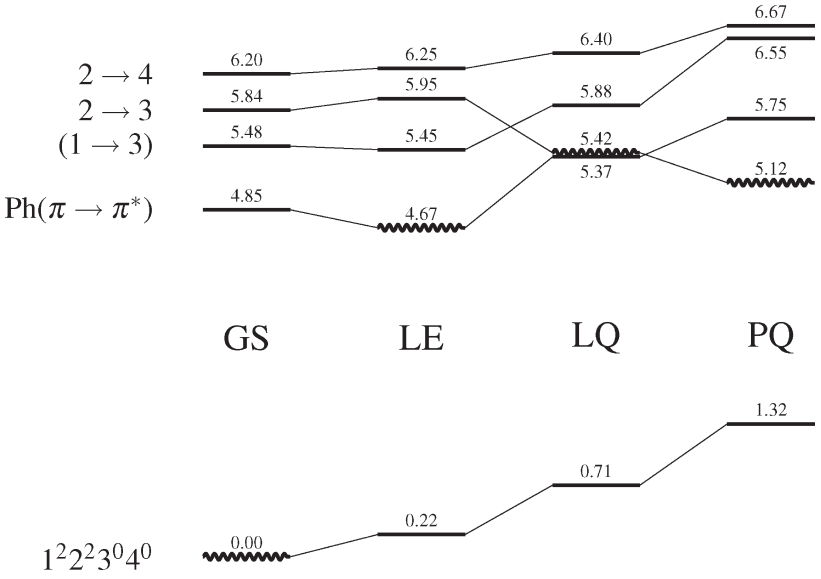

Figure 4. Relative energies (CASPT2(0.25), in eV) of the calculated electronic states of PP in the gas phase at the optimized geometries. The state for which each geometry is optimized is drawn as a wavy line. States of equivalent electron configuration are joined by lines. For the nature of the different states, labeled on the left, refer to Table 3, Figure 3, and the corresponding text.

Table 8. Vertical Absorption Energies (in eV), Dipole Moments (in D), and Oscillator Strengths for the PP Molecule in Acetonitrile at the GS Geometry[a]

	vertical energies			
	CASPT2(0.25)	exp.[10]	μ	f
S_0			1.96	
S_1	4.89		1.22	0.003
S_2	5.55	4.91	−2.41	0.413
S_3	5.96		−6.26	0.014
S_4	6.38		−9.48	0.037

[a] The negative sign in the dipole indicates the negative charge is displaced towards the phenyl ring.

Table 9. Vertical Emission Energies (Transitions to S_0, in eV), Dipole Moments (in D), and Oscillator Strengths for the PP Molecule in Acetonitrile[a]

	vertical energies			
	CASPT2(0.25)	μ	f	ΔG
LE (S_1)	4.47	0.56	0.005	4.68
PQ (S_1)	3.02	−11.92	0.000	4.86
LQ (S_1)	3.95	−10.79	0.004	5.03
BQ (S_1)	3.31	−10.91	0.002	4.86

[a] ΔG is the relative free energy (in eV) with respect to S_0 at the ground state minimum, GS. The negative sign in the dipole indicates the negative charge is displaced towards the phenyl ring.

As with the absorption, there is very little change in the emission at the LE geometry, something that is also observed experimentally for the LE band (4.05 eV in CH_3CN,[10] 4.10 eV in the gas phase).

The most interesting results are obtained by comparing the emissions from the ICT structures. There is a large variation in the transition energies for PQ, LQ, and BQ, of almost 1 eV, and the oscillator strength ranges from practically zero (less than 3×10^{-5}) to approximately the same value as for the LE emission, both quantities increasing in the order PQ < BQ < LQ. The band maximum for the experimentally observed CT band in acetonitrile is located at 3.48 eV; this would agree (considering the overestimation of the transition energies with CASPT2(0.25) already discussed) with the LQ emission, the emissions for PQ and BQ being too low.

The relative free energy of the states at their respective structures is listed in the ΔG column. A scheme of the energies of the first five states for each structure is shown in Figure 5. The three ICT structures have a similar energy, well below S_2 at GS and comparable to S_1, and are therefore accessible from the initial excitation of the molecule; they are also very close to the energy of the fluorescing LE state.

The almost constant energy from LQ to BQ and PQ indicates that the free energy surface is probably very flat between these structures, and fluorescence would be more likely wherever the oscillator strength for the $S_1 \rightarrow S_0$ transition is larger. This would favor emission at LQ and BQ, while the PQ geometry, although energetically available, would give rise to almost no fluorescence.

Druzhinin et al.[10] have estimated some thermodynamic quantities for the PP system from the fluorescence properties; in particular, they conclude the free energy difference between the emitting LE and ICT states is lower than 1 kcal/mol in acetonitrile at room temperature. Our results yield an ICT state about 4 kcal/mol (0.18 eV) higher in energy than the LE state; considering the errors, approximations and assumptions in the experiments, interpretations, and calculations, there is qualitative agreement with the recent experimental findings.

It is interesting that the best accord with the experimental fluorescence is obtained for the LQ structure, which is not a true minimum in our calculations. This could be due to a limitation in the calculation level used in this work, and it is possible that by including a more complete description in the quantum calculations a true minimum with lower relative energy would be

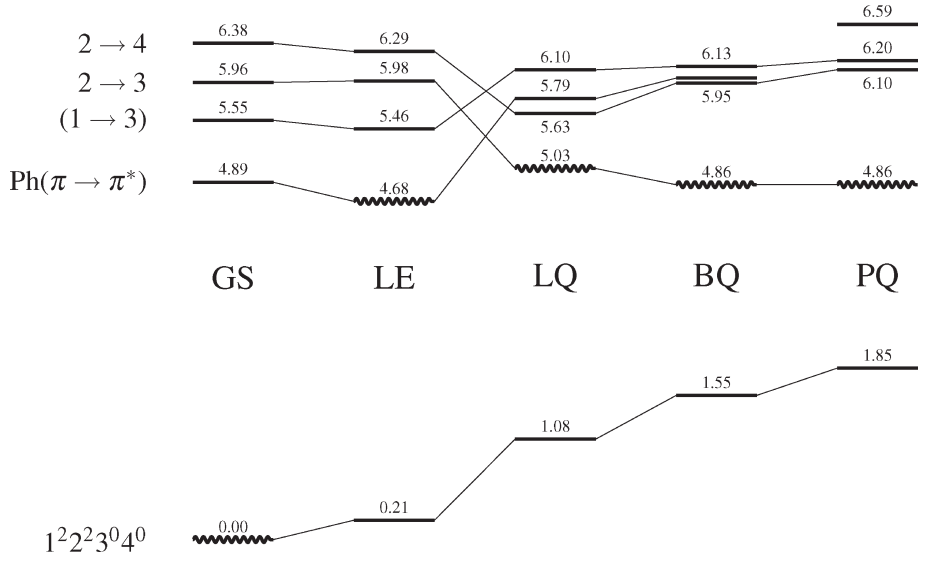

Figure 5. Relative free energies (CASPT2(0.25), in eV) of the calculated electronic states of PP in acetonitrile solution at the optimized geometries. The state for which each geometry is optimized is marked as a wavy line; this is also the state with which the solvent is in equilibrium. States of equivalent electron configuration are joined by lines. For the nature of the different states, labeled on the left, refer to Table 8 and Figure 3.

obtained. On the other hand, the experimental fluorescence band maximum need not correspond to a minimum in the excited state surface, and other elements such as the system's dynamics and the Franck−Condon factors should be included. Some of these considerations favor the fluorescence at an LQ-like structure. First, as pointed out above, the oscillator strength for the electron transition is higher at LQ than at BQ or PQ. Also, the overall molecular shape in LQ is more similar to GS and LE; this means that the structure can be reached with less important solvent reorganization around the solute, while for reaching BQ or PQ more significant solvent changes are needed.

To investigate this suggestion, we optimized the ICT state keeping the solvent frozen in equilibrium with the ground state. The result was a geometry practically identical to LQ in the gas phase, and the transition energy was very similar as well (4.80 eV). It indicates, nevertheless, that the frozen solvent does not pose significant electrostatic or steric impediments to the solute's attaining a geometry close to LQ. When afterward the solvent geometry is relaxed and the solute and solvent are mutually equilibrated, as we mentioned above, the solute geometry proceeds by first keeping the ϕ angle around 180°, and only later is the molecule bent.

In another calculation, the solute geometry was fixed at GS, and the solvent was equilibrated with the active absorption state (identified by its large oscillator strength, initially S_2). In this situation, S_0 and S_1 are destabilized by 0.33 eV and 0.20 eV, respectively, while S_3 and S_4 are stabilized by 0.36 eV and 0.61 eV. This is expected given the orientation and magnitude of the dipole moments of the states. The result is that the S_2 and S_3 states become almost degenerate, but the S_1 state still corresponds to a local excitation.

Considering the above two calculations together, it can be concluded that the solvent's direct influence alone is not sufficient to stabilize the ICT state below the LE one, and a change in the solute geometry is needed. This change, however, is not necessarily a twist of the two rings (θ angle), the modification of the rings' bond lengths, combined with the solvent equilibraton, being enough to ensure the ICT state becomes the first excited state, S_1.

Xu et al.,[15] in a theoretical study of PP and FPP with a similar computational level to the present work, but using the PCM solvent model, arrived to different conclusions. They report, as we do, a considerably flat energy surface for the ICT state. On this surface, they locate a minimum ICT structure comparable to our PQ and two other structures with linear ϕ angle, planar and twisted (PICT and TICT), with θ equal to 0° and 90°, respectively (these two with symmetry constraints). The solvatochromic shift they obtain with PCM for PQ is about half of what we get (0.30 eV vs 0.78 eV), which may be due to the absence of specific interactions in PCM, or to the different active space used in both calculations. The lower solvent shift in their calculations led Xu et al. to discard the linear structures as responsible for the observed "anomalous" band and to accept the PQ structure as the source of the band, in spite of its fluorescence energy being underestimated and the computed oscillator strength being very small.

4. CONCLUSIONS

We have studied the ground and excited singlet states of 1-phenylpyrrole in the gas phase and in acetonitrile solution, using a high-level quantum method for the electronic structure and an explicit MM model for the solvent. The optimized ground state, GS, and locally excited state, LE, structures provide good agreement with the observed absorption bands and the higher-energy fluorescence band. These states have very low dipole moments and are very weakly affected by the solvent; consequently, the absorption and emission properties show little change between the gas phase and solution.

The case is different for the internal charge transfer state, ICT. We could optimize different geometries for an ICT state, all of them belonging apparently to the same electronic surface (corresponding to a 2 → 3 single excitation, see Figure 3) and featuring a quinoidal deformation in the phenyl ring. In gas phase, the lowest-energy structure has perpendicular rings and a pyramidal C_6 atom, and another minimum was found for a structure more similar to GS, with a small θ angle and a linear ϕ

angle. Both ICT structures are significantly higher in energy than the LE minimum and higher than the Franck−Condon point on absorption too, explaining why no fluorescence from this state is observed in the gas phase.

In acetonitrile solution, the ICT state is stabilized, and its energy becomes similar to the LE minimum. The free energy surface seems very flat from the LQ (linear) to the PQ (perpendicular and bent) structure, which makes emission possible from any point of the path. In this direction of geometry change, the emission energy decreases, but so does the oscillator strength, which gives a measure of the probability of transition. Thus, fluorescence is more likely in earlier structures, closer to LQ, where the solute molecule remains linear and with a low twist, and without requiring a large reorganization of the solvent.

Our proposal for the dual florescence in 1-phenylpyrrole is therefore that there are several ICT geometries accessible in polar solvents. The twist between the two rings is not necessary to stabilize the ICT state; the needed changes are the quinoidal deformation of the phenyl and the solvent equilibration with the charge transfer state. The fact that ICT fluorescence is more likely in geometries near LQ can explain why this fluorescence is relatively more intense in the planar and rigidized fluorazene: part of the ICT population of PP can change the geometry and relax through other paths, something that cannot happen in fluorazene.

AUTHOR INFORMATION

Corresponding Author
*E-mail: jellby@unex.es.

ACKNOWLEDGMENT

This work was supported by the CTQ2008-06224/BQU Project from the Ministerio de Ciencia e Innovación of Spain and the PRI08A056 Project from the Consejería de Economía, Comercio e Innovación of the Junta de Extremadura. I.F.G. acknowledges the Junta de Extremadura and the European Social Fund for financial support; A.M.-L. acknowledges financial support from the Juan de la Cierva subprogramme of the Ministerio de Ciencia en Innovación of Spain. The authors also thank the Fundación Computación y Tecnologías Avanzadas de Extremadura (COMPUTAEX) for additional computational resources.

REFERENCES

(1) Lippert, E.; Lüder, W.; Moll, F.; Nägele, W.; Boos, H.; Prigge, H.; Seibold-Blankenstein, I. *Angew. Chem.* **1961**, *73*, 695–706.
(2) Grabowski, Z. R.; Rotkiewicz, K.; Rettig, W. *Chem. Rev.* **2003**, *103*, 3899–4032.
(3) Kato, S.; Amatatsu, Y. *J. Chem. Phys.* **1990**, *92*, 7241–7257.
(4) Hayashi, S.; Ando, K.; Kato, S. *J. Phys. Chem.* **1995**, *99*, 955–964.
(5) Serrano-Andrés, L.; Merchán, M.; Roos, B. O.; Lindh, R. *J. Am. Chem. Soc.* **1995**, *117*, 3189–3204.
(6) Sudholt, W.; Arnulf Staib, A. L. S.; Domcke, W. *Phys. Chem. Chem. Phys.* **2000**, *2*, 4341–4353.
(7) Mennucci, B.; Toniolo, A.; Tomasi, J. *J. Am. Chem. Soc.* **2000**, *122*, 10621–10630.
(8) Minezawa, N.; Kato, S. *J. Phys. Chem. A* **2005**, *109*, 5445–5453.
(9) Yoshihara, T.; Druzhinin, S. I.; Zachariasse, K. A. *J. Am. Chem. Soc.* **2004**, *126*, 8535–8539.
(10) Druzhinin, S. I.; Kovalenko, S. A.; Senyushkina, T. A.; Demeter, A.; Zachariasse, K. A. *J. Phys. Chem. A* **2010**, *114*, 1621–1632.
(11) Parusel, A. B. J. *Phys. Chem. Chem. Phys.* **2000**, *2*, 5545–5552.
(12) Proppe, B.; Merchán, M.; Serrano-Andrés, L. *J. Phys. Chem. A* **2000**, *104*, 1608–1616.
(13) Zilberg, S.; Haas, Y. *J. Phys. Chem. A* **2002**, *106*, 1–11.
(14) Schweke, D.; Baumgarten, H.; Haas, Y.; Rettig, W.; Dick, B. *J. Phys. Chem. A* **2005**, *109*, 576–585.
(15) Xu, X.; Cao, Z.; Zhang, Q. *J. Phys. Chem. A* **2006**, *110*, 1740–1748.
(16) Sánchez, M. L.; Aguilar, M. A.; Olivares del Valle, F. J. *J. Comput. Chem.* **1997**, *18*, 313–322.
(17) Fdez. Galván, I.; Sánchez, M. L.; Martín, M. E.; Olivares del Valle, F. J.; Aguilar, M. A. *Comput. Phys. Commun.* **2003**, *155*, 244–259.
(18) Aguilar, M. A.; Sánchez, M. L.; Martín, M. E.; Fdez. Galván, I. An Effective Hamiltonian Method from Simulations: ASEP/MD. In *Continuum Solvation Models in Chemical Physics*, 1st ed.; Mennucci, B., Cammi, R., Eds.; Wiley: New York, 2007; Chapter 4.5, pp 580−592.
(19) Fdez. Galván, I.; Sánchez, M. L.; Martín, M. E.; Olivares del Valle, F. J.; Aguilar, M. A. *J. Chem. Phys.* **2003**, *118*, 255–263.
(20) Okuyama-Yoshida, N.; Nagaoka, M.; Yamabe, T. *Int. J. Quantum Chem.* **1998**, *70*, 95–103.
(21) Zwanzig, R. W. *J. Chem. Phys.* **1954**, *22*, 1420–1426.
(22) Fdez. Galván, I.; Aguilar, M. A.; Ruiz-López, M. F. *J. Phys. Chem. B* **2005**, *109*, 23024–23030.
(23) Roos, B. O.; Taylor, P. R.; Siegbahn, P. E. M. *Chem. Phys.* **1980**, *48*, 157–173.
(24) Andersson, K.; Malmqvist, P.-Å.; Roos, B. O.; Sadlej, A. J.; Wolinski, K. *J. Phys. Chem.* **1990**, *94*, 5483–5488.
(25) Andersson, K.; Malmqvist, P.-Å.; Roos, B. O. *J. Chem. Phys.* **1992**, *96*, 1218–1226.
(26) Ghigo, G.; Roos, B. O.; Malmqvist, P.-Å. *Chem. Phys. Lett.* **2004**, *396*, 142–149.
(27) Jorgensen, W. L.; Maxwell, D. S.; Tirado-Rives, J. *J. Am. Chem. Soc.* **1996**, *118*, 11225–11236.
(28) Karlström, G.; Lindh, R.; Malmqvist, P.-Å.; Roos, B. O.; Ryde, U.; Veryazov, V.; Widmark, P.-O.; Cossi, M.; Schimmelpfennig, B.; Neogrady, P.; Seijo, L. *Comput. Mater. Sci.* **2003**, *28*, 222–239.
(29) Refson, K. *Comput. Phys. Commun.* **2000**, *126*, 310–329.
(30) Schaftenaar, G.; Noordik, J. H. *J. Comput.-Aided Mol. Des.* **2000**, *14*, 123–134.
(31) Fabian, W. M. F. *J. Comput. Chem.* **1988**, *9*, 369–377.
(32) He, R.-X.; Li, X.-Y. *Chem. Phys.* **2007**, *332*, 325–335.
(33) Rettig, W.; Marschner, F. *Nouv. J. Chim.* **1983**, *7*, 425.
(34) Okuyama, K.; Numata, Y.; Odawara, S.; Suzuka, I. *J. Chem. Phys.* **1998**, *109*, 7185–7196.
(35) Fdez. Galván, I.; Martín, M. E.; Aguilar, M. A. *J. Chem. Theory Comput.* **2010**, *6*, 2445–2454.
(36) Köhn, A.; Hättig, C. *J. Am. Chem. Soc.* **2004**, *126*, 7399–7410.
(37) Schweke, D.; Haas, Y.; Dick, B. *J. Phys. Chem. A* **2005**, *109*, 3830–3842.
(38) Fdez. Galván, I.; Martín, M. E.; Muñoz-Losa, A.; Aguilar, M. A. *J. Chem. Theory Comput.* **2009**, *5*, 341–349.
(39) Sarkar, A.; Chakravorti, S. *Chem. Phys. Lett.* **1995**, *235*, 195–201.
(40) Valsson, O.; Filippi, C. *J. Chem. Theory Comput.* **2010**, *6*, 1275–1292.
(41) Schweke, D.; Haas, Y. *J. Phys. Chem. A* **2003**, *107*, 9554–9560.
(42) Yoshihara, T.; Druzhinin, S. I.; Demeter, A.; Kocher, N.; Stalke, D.; Zachariasse, K. A. *J. Phys. Chem. A* **2005**, *109*, 1497–1509.
(43) Belau, L.; Haas, Y.; Rettig, W. *Chem. Phys. Lett.* **2002**, *364*, 157–163.